Journal of Turbomachinery. Received July 15, 2019;
Accepted manuscript posted April 21, 2020. doi:10.1115/1.4047784

Deficiencies in the SA Turbulence model for the prediction of the stability boundary in highly loaded compressors

Jose Moreno*
Imperial College London
London, UK
j.moreno17@imperial.ac.uk

John Dodds
Rolls-Royce.plc
Derby, UK
John.Dodds@Rolls-Royce.com

Sina Stapelfeldt
Imperial College London
London, UK
s.stapelfeldt@imperial.ac.uk

Mehdi Vahdati
Imperial College London
London, UK
m.vahdati@imperial.ac.uk

ABSTRACT

Reynolds-averaged Navier-Stokes (RANS) equations are employed for aerodynamic and aeroelastic modelling in axial compressors. Their solutions are highly dependent on the turbulence models for closure. The main objective of this work is to assess the widely used Spalart-Allmaras model suitability for high speed compressor flows. For this purpose, an extensive investigation of the sources of uncertainties in a high-speed multi-stage compressor rig was carried out. The grid resolution near the casing end wall, which affects the tip leakage flow and casing boundary layer, was found to have a major effect on the

stability limit prediction. Refinements in this region led to a stall margin loss prediction. It was found that this loss was exclusively due to the destruction term in the SA model.

INTRODUCTION

During engine development, accurate aerodynamic and aeroelastic prediction of the stability boundaries through the entire operation range of multi-stage compressors is of major importance as it allows early identification of aerodynamic, vibration and noise problems.

The flow behaviour in multi-stage machines is inherently unsteady due to the relative motion between stator and rotor blade rows. Moreover, several loss mechanisms such as end-wall boundary layers, shocks (in high-speed machines), tip leakage flows and hub corner separations are naturally unsteady. In part-speed operation and closer to the stall boundary, this unsteadiness becomes more severe due to stage mismatching, higher flow incidence and ultimately, flow separation. As a result, the flow becomes non-axisymmetric across the annulus and multi-stage full-annulus computations are required for both mechanical and aerodynamic analysis. Unsteady computations of full-annulus multi-stage assemblies are extremely expensive and the use of high-fidelity models such as DNS or LES is not feasible yet. As a result, RANS is still the most used method for this type of studies [1,2].

In RANS, mathematical modelling of turbulence is crucial for closure of the Navier-Stokes equations. However, most of the currently available turbulence models are derived from simple canonical flows which are not representative of the reality in high-speed multi-stage machines. Even when reasonably tuned for Aerodynamic Design Point (ADP) operation, these models are not capable of accurate off-design prediction. As a consequence, flow modelling of operation near the stability boundary presents a great challenge.

In order to improve the current CFD capability for off-design condition prediction, two different categories of modelling inaccuracies should be addressed: physical modelling and numerical uncertainty. The physical modelling errors will arise directly from the models, i.e., the source of uncertainty is related to how well the mathematical set of equations describes the physical features that one is aiming to capture in the flow solution. On the other hand, numerical uncertainty

is independent of the models used. It measures how accurately the set of equations is solved.

Due to its robustness, simplicity and efficiency, the Spalart-Allmaras (SA) model [3] is widely used for RANS modelling. However, as any turbulence model, it has its shortcomings such as premature stall prediction, considerable total pressure loss and prediction of larger separation zones. Due to these limitations, Lee. et. al. [4, 5] derived an improved modified SA model based on the works of Liu et. al. [6] and Li et. al. [7]: the former considered a helicity function in order to increase the eddy viscosity production term and suppress the region of hub corner separation in compressors; the latter considered the effect of the pressure gradient in shock-wave/turbulent boundary layer interaction to locally correct the levels of eddy viscosity present in the flow. Lee's modified version of the model (MSA) was validated for a part-span loaded transonic low-speed fan.

In the current work, the MSA model will be applied to a multi-stage compressor operating at high speed condition. The main objective of this work can be divided in two independent parts:

1. Comparison between the original SA [3] and modified SA model [4, 5] suitability for multi-stage high-speed compressor operation prediction.
2. Identification of the main sources of modelling inaccuracies using RANS with these turbulence models.

This paper is structured in the following way: the first part presents the numerical setup of two different case studies used to meet the objectives outlined above. In the second part, a comparison between two different turbulence models for compressor performance prediction is carried out. Finally, it is identified that most of the numerical modelling shortcomings of these models are linked to the tip leakage flow and casing boundary layer modelling and these features are studied in detail.

NUMERICAL SETUP

Case study 1 - Multi-stage domain

The rig studied in this work is a multi-stage high speed intermediate pressure (IP) compressor rig. It has four stages, one variable inlet guide vane (IGV) and a pre-swirl vane. The stationary

blade rows in the first three stages are variable stator vanes (VSV's). During the first part of this work, all the stages were considered. The numerical model did not include any secondary geometric features such as penny gaps in the VSV's, shroud flows inter blade rows and geometrical fillets. Figure 1 illustrates the rig used in case study 1.

The stability limit prediction in multi-stage machines is mainly dependent on two key flow features: flow unsteadiness and turbulence. Both of these effects were taken into consideration. To investigate the role of unsteadiness, the predictions using unsteady full-annulus sliding plane computations were compared against steady state single passage mixing plane computations. The numerical study regarding turbulence modelling is performed using steady single passage mixing plane computations. The stability boundary is defined to be at the point where the compressor starts to operate on the positive slope of the characteristic [8, 9].

The boundary condition at the inlet was prescribed using total pressure, total temperature and flow angles. The inlet profile was kept the same as the one measured in the experiment. The outflow boundary condition is set via a variable area choked nozzle which is throttled to push the compressor towards the stall boundary.

The datum numerical grid used in the first part of this paper contains approximately 0.3 M points per passage. This grid is unstructured within the passage with a body-fitted two-dimensional O-grid around the blade geometries. The rotor passages have 47 radial grid levels across the blade span with refinements towards the hub and tip. The tip gap/casing boundary layer region was modelled using 6 equally spaced radial layers. The number of radial layers in the stator vanes is 53. The average non-dimensional distance (y_2^+) between the first cell and the solid surfaces of blades, hub and casing is approximately 50, 40 and 130, respectively. Wall function (WF) was used to calculate the wall shear stresses on all the solid boundaries. Figure 2 illustrates the mesh detail of the leading edge near the hub and tip of rotor 4 (R4).

Case study 2 - Last stage domain

In the second stage of this work an extensive grid convergence study is performed where the mesh density and near wall distances to different solid surfaces (hub, blades and casing) are studied independently. The numerical domain contains only the last stage of the machine (R4+S4)

and a fixed area choked nozzle. This domain is selected because it was found in case study 1, that stage 4 is the first stage to suffer from premature stall and this work focus on off-design operation near the aerodynamic stability limit.

To further reduce the computational cost, only one operating point close to the stall boundary is considered (Point 'P3' in Figure 3). The inlet b.c. is kept the same as the one obtained at the R4 inlet from the multi-stage computation, i.e., the inlet boundary profile is the mixing plane total pressure, total temperature, flow angles and eddy viscosity obtained at that specific operating point. The outlet b.c. is set via a fixed choked nozzle.

Flow solver

The numerical solutions presented in this work were obtained using AU3D, a solver which has been developed and validated over the past 25 years [10, 11]. This CFD code is a three-dimensional, time-accurate, viscous and compressible RANS solver. Further details about the flow solver are found in the work of Sayma [12].

AN IMPROVEMENT ON THE SA MODEL

Models overview

The model considered in this paper is the SA model without the trip term ($f_{t1} = 0$) presented in [3]. The eddy viscosity transport equation can be written as:

$$\frac{\partial \tilde{\nu}}{\partial t} + u_j \frac{\partial \tilde{\nu}}{\partial x_j} = Diffusion + Source\ term \tag{1}$$

where $\tilde{\nu}$ is the eddy viscosity, u_j is a velocity component in the j^{th} direction, x_j is a coordinate vector and t is time.

The convective and diffusive terms in this model are derived directly from their classical definitions. On the other hand, the exact form of source term is less clear since it is derived from flows in simplified conditions using empirical observations. The focus in this work is to investigate the source term ability to model turbulence in high-speed multi-stage compressors.

The source term in the SA model can be broken down into two terms: production ($P_{\tilde{\nu}}$) and destruction ($D_{\tilde{\nu}}$). For fully turbulent flows, the production term can be written as a function of vorticity and eddy viscosity present in the flow.

$$P_{\tilde{\nu}} = f(\omega, \tilde{\nu}) \tag{2}$$

Here, ω is the vorticity magnitude. The extra terms in the production term of the original SA model are numerical and empirical corrections in laminar and transition regions which are not considered for the fully turbulent flow computations performed in this paper.

The destruction term can be defined as a function of ratio of the eddy viscosity and the distance of the cell to the closest solid wall (d):

$$D_{\tilde{\nu}} = f((\frac{\tilde{\nu}}{d})^2) \tag{3}$$

This sink term represents the turbulent dissipation of the small eddies in the vicinity of a solid surface and it should be passive in free shear flows.

The SA model was not derived for turbomachinery flows which are characterized by very complicated flow features. To improve the model for their application, Lee et. al. [4] suggested the use of a β function which would be multiplied by the production term in the original SA model. This function is dependent on the flow helicity (H^*) and pressure gradient in the flow direction (P^*). These changes result in a local increase of eddy viscosity in the presence of rotational flows or adverse pressure gradients. The rest of the SA model remains unchanged. The modified production term can be written as:

$$P_{\tilde{\nu}} = \beta(H^*, P^*) f(\omega, \tilde{\nu}) \tag{4}$$

The use of this modified SA model (MSA) has shown promising results in [4, 5, 13] for low-speed fan flow modelling. The constants used for the helicity and pressure functions in this paper are the same as the ones suggested by Lee et. al. in [4].

Aerodynamic Performance.

In this section, the SA/MSA model's suitability for multi-stage high-speed machines at a fixed aerospeed operation is studied in detail. Figure 3 shows the overall normalized pressure ratio and mass flow measured from IGV inlet to S4 outlet and the block normalized pressure ratios and mass flows (measured from IGV inlet to S2 inlet and S2 inlet to S4 inlet).

The results obtained using the MSA model show a slight increase in surge/stall margin compared to the original SA. Both in terms of overall and block performance, it is clear that the MSA model is capable of obtaining a stable numerical solution at slightly lower mass flow and higher pressure ratio. Despite the correct trend of the overall characteristic at this speed, it is also observed that the overall stability margin of this machine is underpredicted which was not the case for the fan test cases used by Lee et. al. [4] to derive the model. For similar values of pressure ratio, a slight overflow is observed both in terms of overall and block aerodynamic performance. The model used here did not include any secondary geometric features (penny gaps, shroud flows, etc.) which may increase the blockage across the compressor. However, the authors acknowledge that future studies are required to confirm this statement.

The block performance analysis suggests that the aerodynamic stability limit is reached in the rear stages of the machine. The measured data shows that the rear stages have the first characteristic to roll over to the positive slope as the compressor mass flow is reduced. This feature is predicted correctly with both models. However, closer to the stall boundary, it shows a different trend of the characteristic relative to the measured data. Neither of the models are capable of capturing the compressor characteristic over its whole range.

In the next step, unsteady whole assembly computations were performed to check if the underprediction of the stability limit was due to the steady assumption. Figure 4 presents the results obtained in terms of rig overall, front and rear stages performance. At this aerospeed, it is observed that the unsteady approach does not improve the aerodynamic stability limit prediction. In

the unsteady computation, when the rig is throttled towards point 'P1' throttle area, it surges. In terms of stage matching, the results are identical in the front stages while slightly higher mass flows are obtained in the rear stages. This comparison shows that, at this aero-speed, turbulence modelling has more influence on the stall prediction than the modelling of flow unsteadiness. The SA and MSA turbulence models were further investigated at the operating point 'P2' (the stability limit of the SA model).

Radial profiles.

Figure 5 illustrates the total pressure profiles at the inlet of stator 3 (S3) and stator 4 (S4). The measured radial profiles were obtained at point 'E1' which has a pressure ratio similar to point 'P2' (Figure 3). The results show a good agreement with the measured data over most of the span. Discrepancies are observed at S3 inlet below 20% span where an under prediction of total pressure is present. The results show a similar circumferentially averaged values across the entire span between the two turbulence models. Despite this fact, at operating condition 'P2', the compressor rig is operating at its aerodynamic stability limit with the SA model and still has not reached the stall point with the MSA model as seen in Figure 3.

In the following the analysis, the rear stages of this compressor are analysed and it is found that S4 is the first blade to stall. Figure 6a and 6b show normalized axial velocity contours on S4 suction surface. The flow streamlines in the proximity of the blade surface are also illustrated. The numerical solutions show inward radial flow migration above 20% span. The highlighted circle in Figures 6a and 6b show a region with flow reversal between 10%-35% span. This region is more pronounced when the SA model is used and explains why the compressor rig can be pushed further towards the stall boundary with the MSA model. The delayed separation at the S4 suction surface using the MSA model can have three different origins:

1. The flow angles have changed at the S4 inlet due to the flow differences in the upstream stages of the compressor.
2. Eddy viscosity at S4 inlet has increased due to the higher production of turbulence accumulated across the compressor.

3. Eddy viscosity in the S4 boundary layer has increased due to the higher production term in the MSA model.

Flow angles.

To determine the cause of the delayed separation, radial profiles of relative whirl angle upstream of R4 and absolute whirl angle upstream S4 are shown in Figures 7a and 7b, respectively. The results show that the difference in incidence angle between the two models is very small across the majority of the span. Close to the casing, the MSA model presents slightly higher incidences upstream of S4 which suggests an earlier separation in the S4 suction surface. This is not consistent with what is shown in Figures 6a and 6b where the SA model shows a larger low momentum region with lower velocities above 90% span relative to the MSA model. Also, the characteristics shown in Figure 3 indicate that the SA model stability limit is reached at higher mass flow. Therefore, it is evident that the S4 incidence angles are not the main drive for the premature stall onset.

Inlet eddy viscosity.

Figure 7c shows the spanwise variation in normalized eddy viscosity at the inlet of S4 for the two turbulence models. Despite the similarity in physical quantities such as velocity and total pressure across the mixing planes, higher levels of turbulence are observed upstream of S4 when MSA model is used. In order to isolate the effect of inlet turbulence on the S4 separation, two extra computations using smaller domain formed by the S4 and nozzle are performed. The imposed inlet boundary condition and selected turbulence model is different between the calculations: in the first, the SA turbulence model is used and the inlet boundary condition at S4 is prescribed using the mixing plane obtained from the single-passage computation using the MSA model. The second setup uses the opposite combination.

Figure 6c and 6d present the normalized axial velocity at the S4 suction surface for the cases stated above. By comparison of the numerical solutions in Figure 6, it is evident that the separation region identified by the circle around 10%-35% span is mainly dependent on the turbulence model used, being larger when the SA model is used. Nonetheless, smaller discrepancies can be

found in the solutions which considered the same turbulence model which indicate that the inlet eddy viscosity influences the flow behaviour on the S4 but it is not the primary reason behind the premature stall when using the SA model.

MSA model effect on eddy viscosity.

Figure 8 shows a comparison of eddy viscosity between the models across the different axial stations of the compressor. The change in the SA source term increases the eddy viscosity predominantly above 80% span. It is possible to observe a decay of eddy viscosity as the flow passes across the stator blade rows while it increases across the rotors. Despite the changes in eddy viscosity, the incidence angles upstream of S4 (Figure 7b) are approximately the same which suggest similar levels of blockage in the rotors.

In the next step, the causes of premature separation were investigated at 90% span and 20% span of S4. These locations show more pronounced flow differences between the models as seen in Figures 6a and 6b. Figures 9a and 9b illustrate the source term intensity in the stator passage at 90% span. An analogous plot is presented in Figures 9c and 9d for 20% span . The results show that the source term becomes more dominant (higher values) in the proximity of solid surfaces which is an expected behaviour in boundary layers. For 90% span, the solution source term registers larger values for the MSA model relative to the SA model which is an effect of the introduced modification in the production term. The eddy viscosity increases in the proximity of the blade surface and the flow remains attached for longer which reduces the inward flow migration on S4 suction surface. As a consequence, the flow separation region between 10%-35% span is reduced as shown in Figures 6a and 6b.

Similar levels of source term are observed for both models near the suction surface trailing edge at 20% span. In this region, the flow is reversed in the solution obtained with the SA model and, as a result, higher levels of turbulence production are expected compared to MSA model. This is not reflected in the results which suggest that helicity and pressure gradient model is capable of a producing a more localized control of eddy viscosity in the non-separated regions.

The delayed separation of the MSA model can hence be attributed to two causes: primarily, to an increase of eddy viscosity in the suction surface of the stator vane and secondly, to the growth

of inflow turbulence due to the cumulative effect across the multi-stage compressor.

The MSA model presents an improvement towards the prediction of the aerodynamic stability limit in high-speed multi-stage compressors as it predicts the stability point closer to the measured data. Nonetheless, it is evident that the SA formulation is not capable of predicting the whole range of compressor operation and it is even more difficult to determine whether it represents the flow physics correctly. For this reason, the numerical and modelling inaccuracies of the SA formulation are investigated in more detail in the following section.

NUMERICAL AND MODELLING INACCURACIES OF THE SA FORMULATION

The first step towards modelling improvement is to reduce the amount of numerical uncertainty present in the model due to numerical diffusion or poorly resolved boundary layers. For this purpose, the numerical domain of case study 2 is used at the operating point 'P3' (Figure 3). The MSA model is selected for this investigation.

An extensive grid convergence study was performed where the mesh density and near wall distances to the different solid surfaces (hub, blades and casing) were considered independently. This study is not presented here, however, the conclusions were as follows:

1. If the near wall distances are kept constant on all the surfaces, for a range of y_2^+ presented in case study 1, the numerical solution was not sensitive to grid resolution change as long as more than 0.3 M points per passage was used. This was investigated by reducing the base grid cell size in all the directions (radially, azimuthal and axial) individually and simultaneously.
2. If the grid resolution is kept constant at 0.3 M points per passage, but it is expanded towards the walls at the hub or blades (lower y_2^+ with similar passage resolution), it is observed that for an average y_2^+ in range between 30 and 70 (WF recommended values), the solutions do not show significant differences.
3. If the same study as in the previous bullet point is performed in the casing region, i.e., the number of layers is increased in the tip gap/endwall region towards a $y_2^+ \sim 30 - 90$ (case study 1 has $y_2^+ \sim 130$), the solution shows a major loss in stall margin.

While findings 1) and 2) are consistent with common practice for the use of WF and turbulence

models, finding 3) raised concerns.

In literature, the number of grid layers which is used for modelling of the endwall boundary layer and tip gap flow varies. The use of 5-12 tip gap layers is common amongst papers which study rotating stall and tip clearance flows [2, 14–16]. Moreover, attempts have been made for compressor prediction using more than 17 layers on the endwall boundary layer region [17, 18]. Common guidelines specify the non-dimensional distance for the no slip condition as $y_2^+ < 1 - 5$.

The work of Zante et al. [19] is often used as a reference for tip clearance flows where he showed that the use of 12 layers is accurate enough for modelling of endwall boundary layer and tip leakage flow. This work also demonstrated that the role of the wall bounded shear layer (WBSL) is of great importance towards accurate modelling of stability limits in compressors. Depending on the relative velocity difference between the tip leakage flow jet and the casing, different shear strength will be observed and the stability limit will differ. Obviously, depending on the turbulence model, operating condition and geometry, the modelling requirements will differ. A generic model which gives a correct trend and accurate prediction of compressor performances is still sought. The aim of the next section is to examine the importance of near wall refinement and grid density in the tip region. This will narrow down the sources of uncertainty in the SA formulation.

End-wall boundary layer modelling uncertainty study.

In order to evaluate the grid requirements to obtain a mesh independent solution two different sources of uncertainties were considered:

1. "*Discretization error*" given by the grid density in the endwall boundary layer region. This is the numerical uncertainty that arises from the transformation of a continuous set of partial differential equations into a discrete algebraic system. It depends on the scheme and methods used (finite-volume, finite-differences, etc.) and should decrease as the grid is refined.
2. "*Boundary layer modelling error*" near the end wall region. This source of uncertainty is an error in the physical modelling of turbulence and/or WF.

It is clear that both error sources are related to the grid resolution: the first one is directly related to the mesh base size while the latter is simultaneously dependent on mesh resolution and models

applied. This is because increasing the resolution near the wall decreases the wall distances which has an impact on WF and turbulence model source term. In order to clearly differentiate between the two, the terminology "*discretization error*" and "*modelling error*" is used.

Discretization error.

The first step was to evaluate the quality of the solution in terms of grid independence. For this purpose, 5 grids with different number of layers in the casing region were tested. The number of layers in the tip gap/casing region for each grid is listed in table 1 (Grids A-E). Figures 10a and 10b illustrate the differences between grid B and D.

In order to isolate *discretization error* from the *modelling error*, a preliminary set of computations was performed where the casing was modelled as a slip wall. The blade tip was still modelled as a viscous wall. This treatment only neglects the casing shear stress on the fluid but resolves the tip leakage flow and its interaction with the main passage flow. Figure 11a compares the R4 operating point predictions considering an inviscid casing for grids A-E. Also shown in this plot is the R4 characteristic from case study 1. The results in terms of overall pressure ratio and mass flow are the same for all grids, which shows that only two layers are sufficient if the losses due to the casing wall are not considered.

Boundary layer modelling error.

In the second step of this study, the effect of the above grid refinements on a non-slip wall with WF is investigated. As before, grids A-E were tested. Figure 11b shows the predicted normalized mass flow against the normalized pressure ratio obtained for the same exit nozzle area as before. The results show that the total pressure ratio decreases if the number of grid layers in the end-wall region is increased. Also, the predictions of grid D and E are very close to each other which indicates that the solution is grid independent if more than 19 layers are used. Note that for grids D and E, y_2^+ values are within the theoretical range for the use of zero pressure gradient WF ($90 > y_2^+ > 30 \sim 50$).

Figure 12 illustrates the flow for the different grids in terms of relative axial velocity in a radial plane at 98.5% span. This is a radial plane which intersects the rotor tip. The tip leakage flow

reversal area changes depending on the grid. As the grid is refined, the tip leakage flow is pushed forward in the passage and the amount of reversed flow increases. As a consequence, the flow blockage is higher and the total pressure ratio drops for the same operating point. Furthermore, the flow separation in the casing region changes the flow pattern downstream of the rotor, resulting in higher outflow angles at rotor exit.

Figure 13 shows the difference in solutions for grids A-E in terms of radial profiles of total pressure ratio across the entire span and outflow angles above 80% span downstream of R4. The tip clearance refinement has a major effect on the total pressure profiles above 60% span, with higher total pressure predicted for the coarser grids. The results obtained using 2 and 6 layers are very similar which indicate that using a grid with 6 layers does not capture the interaction of the flow with the casing wall. As the grid is refined, higher incidence angles at S4 inlet above 92% span are observed. This is caused by the change in tip leakage flow trajectory in R4 and will result in premature stall of S4.

Wall distance limitation.

The previous sections have shown that a grid independent solution is achieved with 19 layers in the tip gap region as long as WF is used. However, the use of WF in this context is questionable as it assumes that the velocity profile is similar to a flow at zero pressure gradient. In order to test this assumption, the casing boundary layer was resolved using grid F. Figure 14 shows the results from grid F compared with the grid E (finest grid with WF) and R4 characteristic. Both the R4 performance and radial profiles are presented in this plot. The results obtained with the two modelling approaches are very similar which demonstrates that the use of WF on the casing does not compromise the compressor aerodynamic performance prediction. It can be concluded that for the current test case, WF presents a good approximation to the no slip boundary condition even in the presence of strong favourable pressure gradient within the gap between the rotor tip and the casing.

The previous comparison has shown that the difference in performance predictions between 2-19 layers seen in Figures 11-13 are not caused by the use of wall functions. The hypothesis is as follows: the SA model and MSA contain a destruction term which is directly dependent on

the cell distance to the closest solid surface, i.e. the dimensional d. By reducing d towards a boundary-layer-resolved solution, the amount of eddy viscosity in the boundary layer is reduced, which enhances flow separation in the casing region leading to high levels of total pressure loss.

To examine this hypothesis, a new grid (Grid G) was generated with the same minimum near wall distance (dimensional y_2) as grid B (6 layers). However, the level of refinement in the end wall region was kept similar to Grid E. Figure 10c shows the configuration of grid G. Figure 15 shows the results obtained in terms of R4 aerodynamic performance and radial profiles of total pressure. Results obtained using grid G shift the operating point back towards the result obtained with the grid B. It can be concluded that, regardless of the boundary condition applied on the casing, the total pressure loss is dependent on the value ofy_2, the dimensional distance between the first cell and the casing wall.

These findings are not surprising since the SA model was not designed for near wall modelling of tip leakage and end wall shear layer interaction. However, a common assumption amongst industry and scientific community is that grid refinements for well resolved boundary layers result in an accuracy improvement when using the SA model in high-speed compressor flows. The results presented in this section suggest that when y_2 value is decreased below a certain threshold, the destruction term is over predicted. Consequently, refined tip gaps/casing end walls leads to poor performance predictions. This is particularly important for the current test case which is a high-speed rotor with tip gaps of 1.5$\%$ blade span and the relative velocity difference between the casing and blade tip is very large. The effect of the under prediction of eddy viscosity in the casing region can become less relevant for low-speed machines and smaller tip gaps as suggested in [19].

The next section will test the effect of the destruction term in a multi-stage compressor and present a comparison against compressor performance measured data.

Multi-stage effects.

To obtain a multi-stage grid independent solution, the grid D configuration was used through the entire rig. The rig performance obtained at 100$\%$ aerospeed is presented in Figure 16 which compares the measured characteristics with numerical solutions obtained using grids B and D. The block 4 characteristic is measured from S3 inlet to S4 inlet. The stability limit is reached at

stator 4 for both grids. As before, a loss in stall margin is evident when the casing boundary layer is well resolved (grid D).

Figure 17 presents the differences in incidence angles between grid D and grid B plotted against span. The flow pattern on the S4 suction surface when using grid D at operation point 'P3' (see Figure 16) is also shown in this plot. Figure 17a shows that for the same nozzle area, grid D registers an increase in the incidence angle above 70% span relative to grid B. Moreover, for the solution obtained with grid D at operating point 'P3', the flow reverses on the S4 suction surface as shown in Figure 17b. Comparing the solution obtained with grid D at operating condition 'P3' with the solution obtained with grid B at operating condition 'P2' (illustrated in Figure 6b), it is evident that S4 is operating closer to stall with grid D since above 70% span, grid D shows a larger separation zone relative to grid B. It is important to note that the solution shown in Figure 6b is obtained at operating point 'P2' which has a lower nozzle area than 'P3' which indicates that the stability boundary with grid D is obtained at higher mass flows. It is also observed that radial flow migration between 10%-35% span is no longer present. The larger separation region above 70% span increases the casing end wall blockage and the incidence at lower span heights decreases (due to higher mass flow at these heights) as shown in Figure 17a. The aforementioned observations suggest that the effect of grid refinement on the rotors is cumulative across the stages leading to further performance deterioration as the number of stages in the compressor increases or the stall onset moves towards the back stages of the compressor.

In order to isolate the wall distance effect on multi-stage arrangements and determine the effect of this term on the rotor casing flow, two extra computations were performed. In these, the computational grids B and D were used and the MSA model destruction term was set to zero in the cells which considered the rotor casing as the closest surface. The original formulation of the MSA model was kept in stator blade rows. Figure 18 shows the results obtained. The differences between the characteristics for the coarse (Grid B) and the fine grid (Grid D) are minor with this formulation of the MSA. Minor discrepancies can be observed for 'P1' throttle area where different operating points are obtained.

DISCUSSION ON CASING FLOW TURBULENCE MODELLING

From the results presented throughout this paper, it is clear that the SA model formulation is not capable of capturing the entire characteristic accurately in high-speed compressors. Furthermore, it is also observed that the stall boundary is closer to the experiment when using a coarser grid or neglecting the SA destruction term in the vicinity of the casing. This section aims to give a qualitative analysis of the tip gap flow physics in high-speed compressor flows and relate it to the SA formulation. It also aims to establish a 'best practice' when using this model.

Destruction term dependence.

Figure 19a and 19c show the normalized eddy viscosity at an axial cut at 50% chord of R4 with grids B and D, respectively. A similar plot is presented in 19e where grid D is used and the destruction term is neglected for the cells which consider the casing as the closest surface.

In the end wall region, there is a clear difference between results. When the destruction term is considered in this region, grid D shows lower values of eddy viscosity than grid B (Figures 19a and 19c). The reduction in eddy viscosity enhances the flow separation in the casing region which leads to the high levels of total pressure loss described in the previous sections. When the destruction term is neglected in the casing vicinity, that low eddy viscosity region vanishes (Figure 19e) and the numerical solutions with grids B and D become similar.

Figures 19b,19d and 19f present the MSA model source term corresponding to the cases outlined before. High positive values of source term indicate that the production term is dominant whilst high negative levels indicate that the destruction term is larger. The tip leakage flow can be described in terms of two shear layers: 1) the free shear between the tip leakage flow and the main flow within the passage; 2) the wall bounded shear layer (WBSL) due to the interaction between the jet and the casing. All of the solutions in Figure 19 show that the production term is more pronounced in the region where the tip leakage jet interacts with the main flow in the passage. Furthermore, as the flow approaches the gap, a turbulence decay is observed. This is a result of the tip clearance flow being predominantly inviscid, driven by the pressure gradient between the pressure and suction surfaces of the blade as previously suggested in [9, 20].

When analysing the results obtained with the MSA formulation (Figure 19b and 19d), the de-

struction term is the dominant term in the region where the tip leakage jet interacts with the casing shear layer. The destruction term dominance is more pronounced for grid D which extends across the entire passage. Therefore, the levels of eddy viscosity drop when grid D is used. Obviously, when the destruction term is not considered in the proximity of the casing, the eddy viscosity destruction does not have an impact on the WBSL modelling (Figure 19f). These observations indicate that the WBSL modelling in the SA formulation has a significant destruction term dependence.

Flow physics.

To understand why the differences between grids B and D in Figure 16 become larger as the compressor is pushed towards the stability limit, the flow physics of the tip leakage jet are discussed in this section. In compressor flows, when viewed from the rotors frame of reference, the compressor casing is rotating at constant speed in direction of the tip leakage jet. Figure 20a presents a 2D sketch which illustrates the effect of the casing rotation on the tip leakage jet and its interaction with the casing shear layer for near stall (red) and design (blue) conditions. Figure 20b presents a 2D illustration of an axial cut in a blade passage which shows the jet velocity profiles near the casing wall. The WBSL strength is highly dependent on the velocity difference between the tip leakage jet and the casing velocity [19]. As the compressor loading increases, the pressure difference between pressure and suction surfaces of the blade increases. As a result, the jet velocity increases, the tip leakage flow is pushed upstream and the WBSL becomes stronger.

Figure 21 shows a decomposition of the different terms of the eddy viscosity equation for an equilibrium turbulent boundary layer. The δ_* is the boundary layer displacement thickness. It is evident that when finer grids are used (small d), the eddy viscosity transport in the SA model formulation is dominated by destruction. Additionally, grid refinements towards the casing wall will approximate the velocity of the casing closest cells to the rotational speed of the surface. Because of a reduction in velocity difference between the jet an the wall velocity, the turbulence production in this region is inevitably reduced. These effects point towards a reduction in eddy viscosity in the casing boundary layer and promotion of separation when finer grids are used. Due to flow separation from the casing, the δ_* of the boundary layer in the casing region increase further. As

a consequence, instead of generating turbulence due to the interaction between the jet and the casing, the model decreases the eddy viscosity, which appears to be over-dissipative for this type of flows. For high values of y_2^+, the destruction term does not play a significant role which results in higher levels of turbulence near the casing and the flow separation is delayed.

The results presented in this paper suggest that eddy viscosity levels near the casing end wall should be higher than what is predicted by the model. When using the fine grid, despite the existence of a high shear between the tip leakage jet and the casing wall, the levels of turbulence do not increased. Based on the results obtained here, the authors suggest neglecting the near casing destruction term when using the SA model for modelling of highly loaded compressors. In this approximation, it is assumed that the turbulent dissipation on the casing walls is negligible when compared with the eddy viscosity production due to the WBSL.

A tip gap flow comparison against measured data to validate the results obtained in this work is currently not available. In future studies, high fidelity simulations (DNS) will be used to improve the SA modelling of WBSL in high speed compressor flows.

CONCLUSIONS

In this work, an extensive study of the SA and MSA turbulence models' behaviour in a high-speed multi-stage compressor is performed. Numerical and physical modelling uncertainties of the SA formulation are investigated. The following conclusions are obtained from this work:

- The MSA model presents several benefits regarding the turbulence modelling in compressors. The flow solutions show higher levels of turbulence in more localized separation regions. As a consequence, numerical solutions closer to the stability limit are obtained.
- The use of the SA and its modifications for tip leakage flow turbulence modelling result in an underprediction of eddy viscosity near the casing. This results in premature flow separation and ultimately compressor stall.
- Neglecting the effect of the destruction term in the MSA formulation in cells which consider the casing as the closest surface (only on rotor blade rows) shows an improvement in the prediction of constant aerodynamic speed characteristics.
- The issues raised in this work regarding the use of the SA model in turbomachinery are more relevant for multi-stage arrangements. In a single stage arrangement, the interaction between the casing and tip leakage flow will not affect the flow behaviour of blade rows located downstream and therefore, it might not compromise the stall margin prediction to the same extent.

ACKNOWLEDGEMENTS

The authors would like to acknowledge Rolls-Royce.plc for supporting and funding this study. They would also like to thank their colleagues at Imperial College London for very useful discussions.

NOMENCLATURE

ADP Aerodynamic design point

IP Intermediate pressure

VSV Variable stator vanes

WBSL Wall bounded shear layer

WF Wall function

$\bar{m}$ Corrected inlet mass flow

d Distance between a cell and the nearest solid boundary

H^* Normalized helicity

P^* Normalized pressure gradient in the flow direction

t Time

y_2 First cell wall distance

y_2^+ Non-dimensional wall distance

x_j Coordinate vector

u_j Velocity vector

β MSA model function

δ_* Displacement thickness

ω Vorticity magnitude

$\tilde{\nu}$ Eddy viscosity

REFERENCES

[1] Choi, M., Smith, N. H., and Vahdati, M., 2012. "Validation of Numerical Simulation for Rotating Stall in a Transonic Fan". *Journal of Turbomachinery,* **135**(2), nov.

[2] Dodds, J., and Vahdati, M., 2015. "Rotating stall observations in a high speed compressor-part II: Numerical study". *Journal of Turbomachinery,* **137**(5), may.

[3] Spalart, P. R., and Allmaras, S. R., 1992. "One-equation turbulence model for aerodynamic flows". In 30th Aerospace Sciences Meeting and Exhibit, no. 1, pp. 1–21.

[4] Lee, K. B., Wilson, M., and Vahdati, M., 2018. "Validation of a numerical model for predicting stalled flows in a low-speed fan-Part I: Modification of Spalart-Allmaras turbulence model". *Journal of Turbomachinery,* **140**(5), may.

[5] Lee, K. B., Dodds, J., Wilson, M., and Vahdati, M., 2018. "Validation of a numerical model for predicting stalled flows in a low-speed fan-part II: Unsteady analysis". *Journal of Turbomachinery,* **140**(5), may.

[6] Liu, Y., Lu, L., Fang, L., and Gao, F., 2011. "Modification of Spalart-Allmaras model with consideration of turbulence energy backscatter using velocity helicity". *Physics Letters, Section A: General, Atomic and Solid State Physics,* **375**(24), jun, pp. 2377–2381.

[7] Ma, L., Lu, L., Fang, J., and Wang, Q., 2014. "A study on turbulence transportation and modification of Spalart-Allmaras model for shock-wave/turbulent boundary layer interaction flow". *Chinese Journal of Aeronautics,* **27**(2), apr, pp. 200–209.

[8] Day, I. J., and Cumpsty, N. A., 1978. "Measurement and interpretation of flow within rotating stall cells in axial compressors.". *J Mech Eng Sci,* **20**(2), apr, pp. 101–114.

[9] Camp, T. R., and Day, J., 1997. "A study of spike and modal stall phenomena in a low-speed axial compressor". In Proceedings of the ASME Turbo Expo, Vol. 1, ASME, p. V001T03A109.

[10] Vahdati, M., Sayma, A. I., Freeman, C., and Imregun, M., 2005. "On the use of atmospheric boundary conditions for axial-flow compressor stall simulations". *Journal of Turbomachinery,* **127**(2), apr, pp. 349–351.

[11] Vahdati, M., and Cumpsty, N., 2016. "Aeroelastic Instability in Transonic Fans". *Journal of Engineering for Gas Turbines and Power,* **138**(2), feb.

[12] Sayma, A. I., Vahdati, M., and Imregun, M., 2000. "An Integrated Nonlinear Approach for Turbomachinery Forced Response Prediction. Part I: Formulation". *Journal of Fluids and Structures,* **14**(1), jan, pp. 87–101.

[13] Kim, S., Pullan, G., Hall, C. A., Grewe, R. P., Wilson, M. J., and Gunn, E., 2019. "Stall Inception in Low-Pressure Ratio Fans". *Journal of Turbomachinery,* **141**(7), jul.

[14] Pullan, G., Young, A. M., Day, I. J., Greitzer, E. M., and Spakovszky, Z. S., 2015. "Origins and structure of spike-type rotating stall". *Journal of Turbomachinery,* **137**(5), may.

[15] Vo, H., Tan, C. S., and Greitzer, E. M., 2008. "Criteria for spike initiated rotating stall". *Journal of Turbomachinery,* **130**(1), jan.

[16] Cevik, M., Vo, H. D., and Yu, H., 2016. "Casing treatment for desensitization of compressor performance and stability to tip clearance". *Journal of Turbomachinery,* **138**(12), dec.

[17] Nan, X., Lin, F., Wang, S., Liu, L., Ma, N., and Chen, J., 2014. "The analysis of axial momentum of the rotor tip flows for axial compressors with circumferential grooves". In Proceedings of the ASME Turbo Expo, Vol. 2A, American Society of Mechanical Engineers (ASME).

[18] Nan, X., Lin, F., Himeno, T., and Watanabe, T., 2018. "The behavior of the casing boundary layer with the presence of tip leakage vortex". In Proceedings of the ASME Turbo Expo, Vol. 2A-2018, American Society of Mechanical Engineers (ASME).

[19] Van Zante, D. E., Strazisar, A. J., Wood, J. R., Hathaway, M. D., and Okiishi, T. H., 2000. "Recommendations for achieving accurate numerical simulation of tip clearance flows in transonic compressor rotors". In Journal of Turbomachinery, Vol. 122, American Society of Mechanical Engineers Digital Collection, pp. 733–742.

[20] Chen, G. T., Greitzer, E. M., Tan, C. S., and Marble, F. E., 1991. "Similarity analysis of compressor tip clearance flow structure". *Journal of Turbomachinery,* **113**(2), apr, pp. 260–269.

LIST OF FIGURES

LIST OF TABLES

TABLES

Table 1. Grid configurations in the proximity of the casing.

Grid	A	B	C	D	E	F
Number of layers	2	6	12	19	39	156
Casing average y_2^+	500	130	89	55	28	0.65

FIGURES

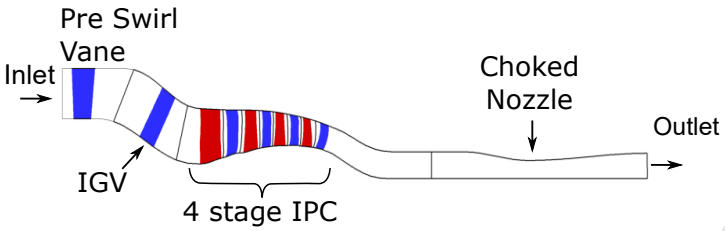

Fig. 1. Compressor rig used in case study 1.

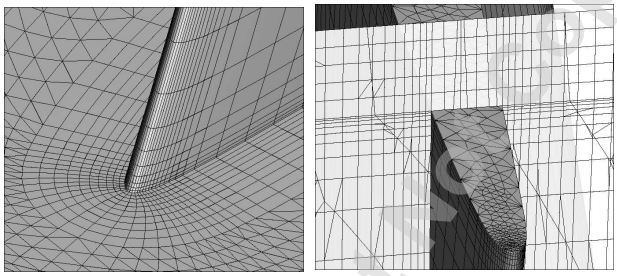

(a) Hub leading edge. (b) Tip gap axial cut.

Fig. 2. Mesh detail of rotor 4.

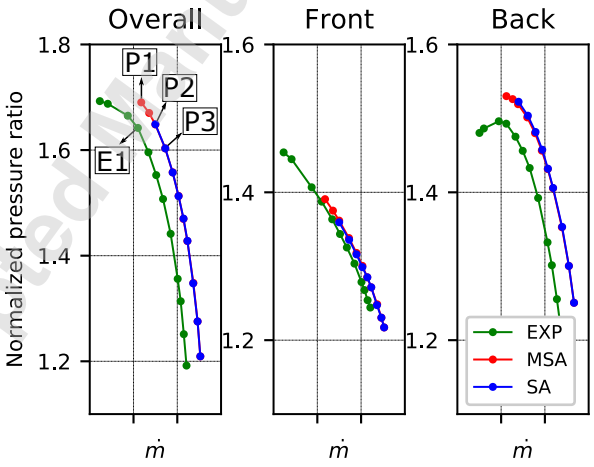

Fig. 3. Steady aerodynamic performance of the compressor rig at 100% aerospeed.

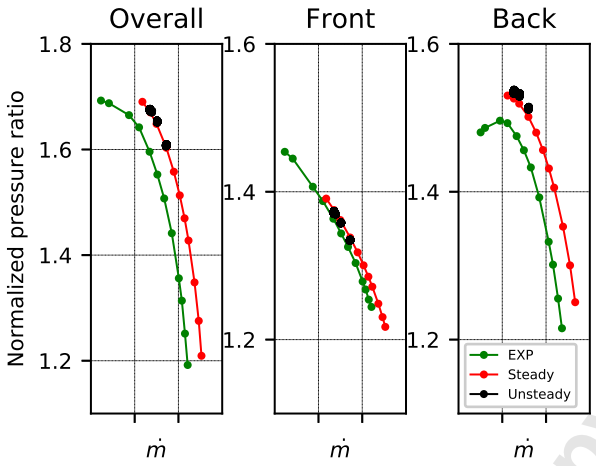

Fig. 4. Comparison between the steady and unsteady aerodynamic performance prediction of the compressor rig using the MSA model.

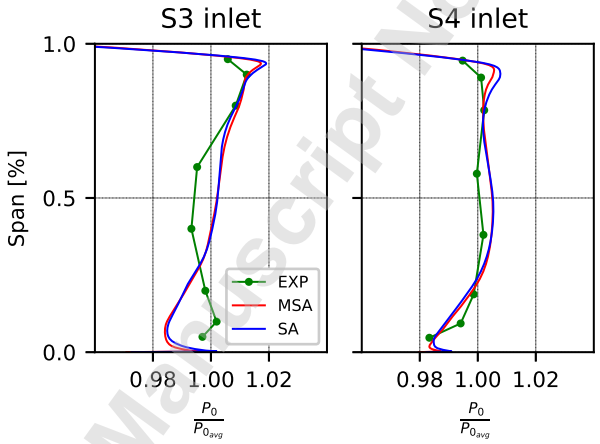

Fig. 5. Radial profiles at operating point 'P2' (CFD) and 'E1' (Measurements).

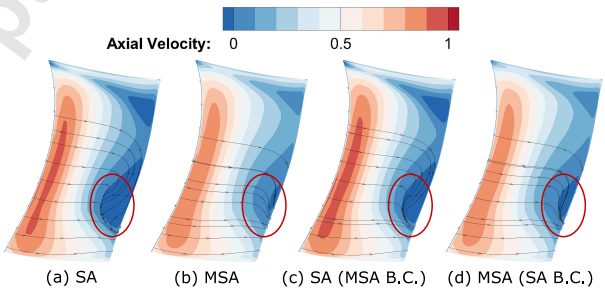

Fig. 6. Normalized axial velocity in the proximity of S4 suction surface (operating point 'P2').

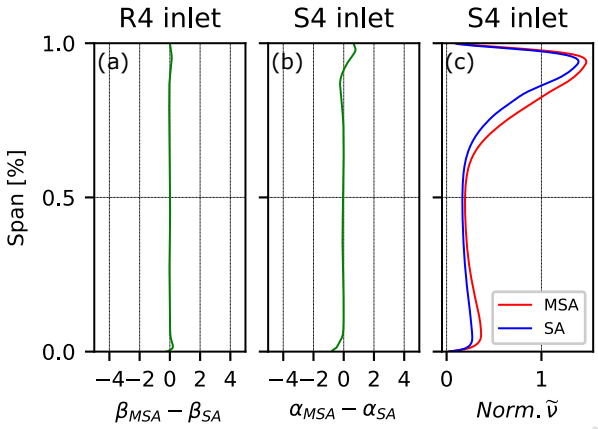

Fig. 7. Comparison of spanwise variation in relative whirl angle upstream of R4 (a), absolute whirl angle upstream of S4 (b) and normalized eddy viscosity upstream of S4 (c) between turbulence models.

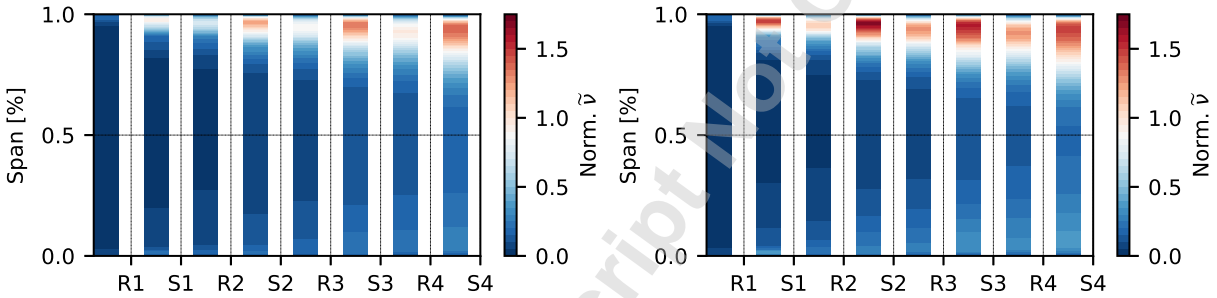

(a) SA model. (b) MSA model.

Fig. 8. Circumferentially averaged radial profiles of eddy viscosity at different compressor axial stations.

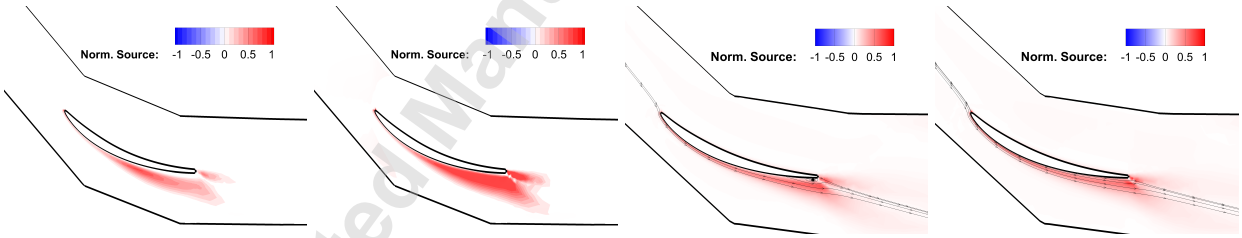

(a) SA Source - 90%. (b) MSA Source - 90%. (c) SA Source - 20%. (d) MSA Source - 20%.

Fig. 9. Normalized source term contour at 90 % and 20% span of the S4 passage.

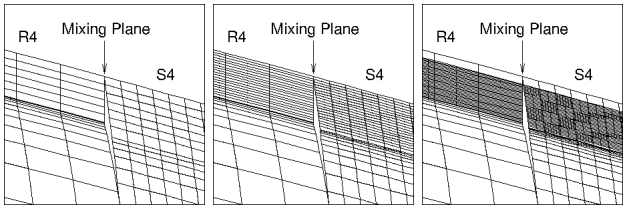

(a) Grid B (b) Grid D (c) Grid G

Fig. 10. Differences between the grids used during case study 2.

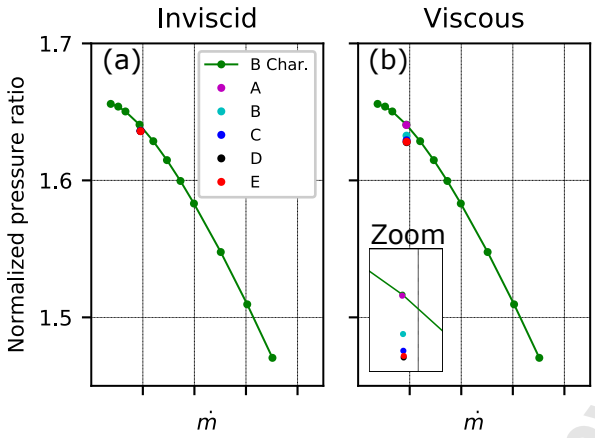

Fig. 11. Comparison between grids at the same operating point using an inviscid (a) and viscous casing boundary condition using WF (b).

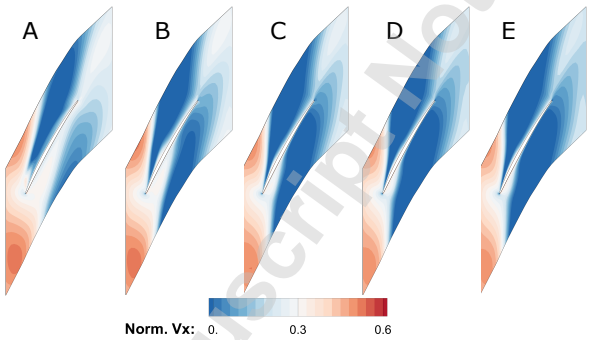

Fig. 12. Grid influence on the normalized axial velocity near the casing surface of rotor 4 ('P3' operating condition).

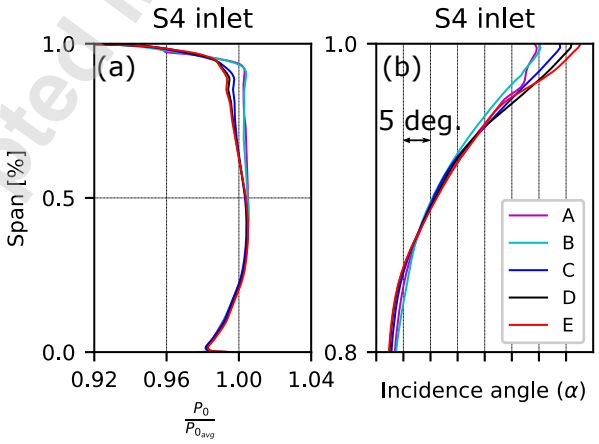

Fig. 13. Spanwise variation of normalized total pressure (a) and incidence angle (b) at the S4 inlet.

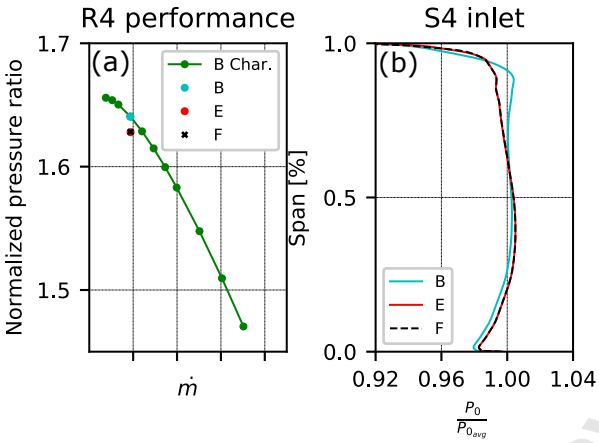

Fig. 14. R4 performance (a) and S4 total pressure inlet profile (b) using grid E and Grid F.

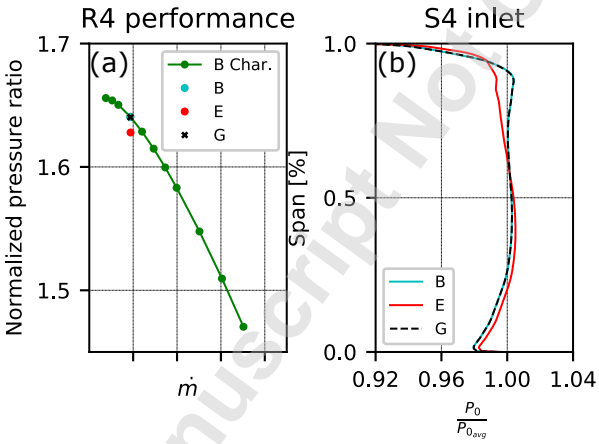

Fig. 15. R4 performance (a) and S4 total pressure inlet profile (b) using grid E and Grid G.

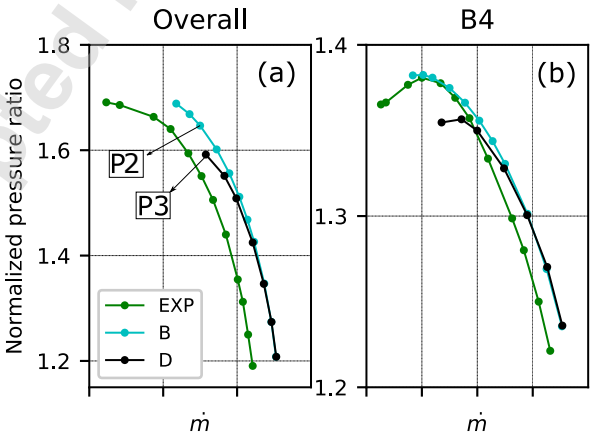

Fig. 16. Compressor rig (a) and B4 (b) aerodynamic performances using grids B and D (MSA model)

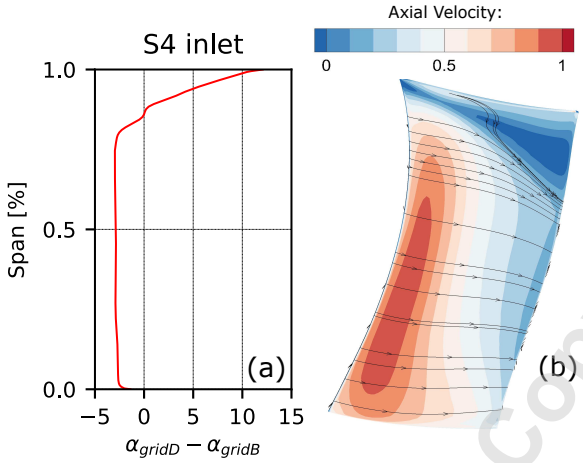

Fig. 17. Difference in incidence angles between grids B and D upstream of S4 at operating point 'P3' (a). Grid D normalized axial velocity in the proximity of S4 suction surface - point 'P3' (b).

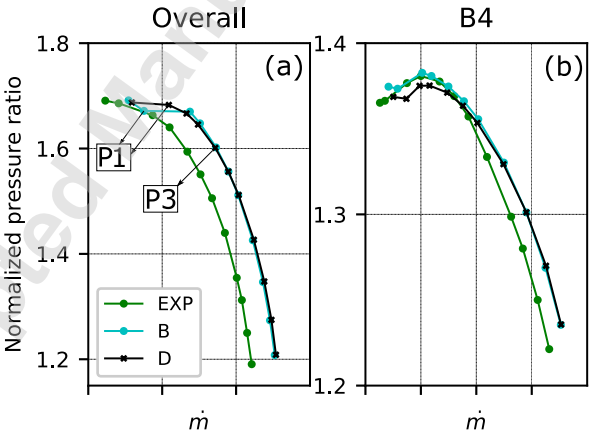

Fig. 18. Compressor rig (a) and B4 (b) aerodynamic performances using grids B and D using the MSA model neglecting the eddy viscosity destruction in the casing surface.

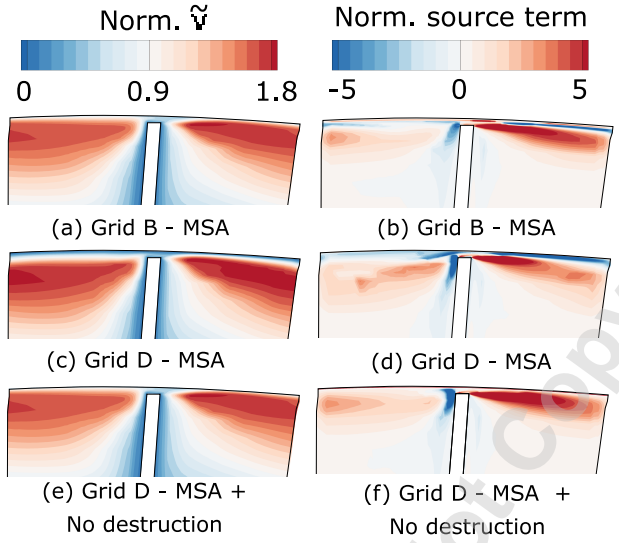

Fig. 19. Comparison between normalized eddy viscosity and source term at operating condition 'P3' for grids B (MSA model) and grid D (MSA model with and without destruction term) - R4 axial cut near tip region at 50% chord.

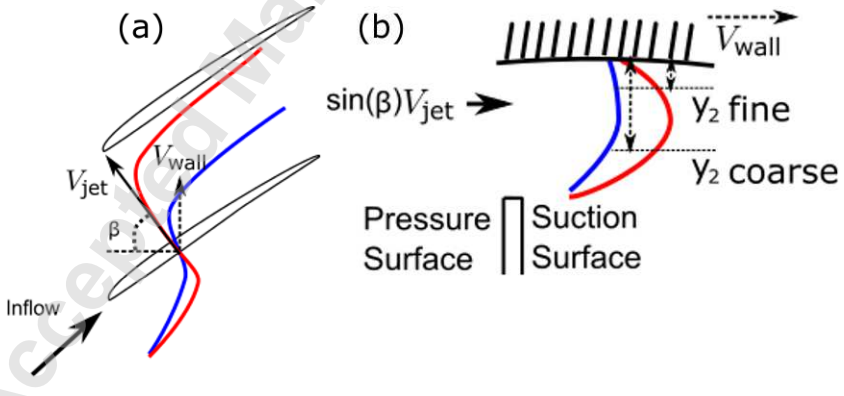

Fig. 20. Effect of tip leakage flow trajectory relative to the casing wall velocity (a) and velocity profile interaction with the WBSL (b). Red and blue represent pre stall and design condition, respectively.

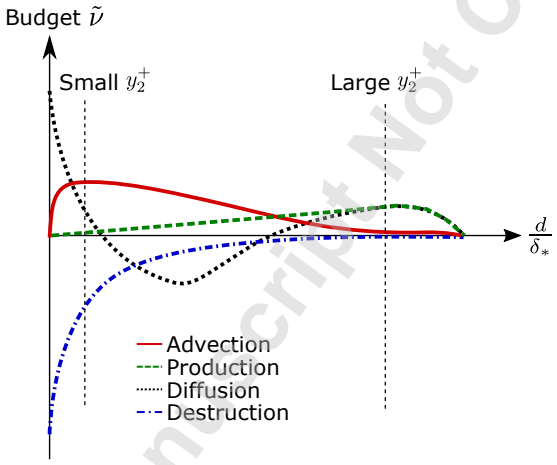

Fig. 21. Eddy viscosity budget for a flat plate boundary layer.